Vertical silver@silver chloride core-shell nanowire array for carbon dioxide electroreduction

Ge, Junyu; Long, Jun; Sun, Zixu; Feng, Han; Hu, Jie; Koh, See Wee; Yu, Qing; Xiao, Jianping; Li, Hong

2019

Ge, J., Long, J., Sun, Z., Feng, H., Hu, J., Koh, S. W., . . . Li, H. (2019). Vertical silver@silver chloride core-shell nanowire array for carbon dioxide electroreduction. ACS Applied Energy Materials, 2(9), 6163-6169. doi:10.1021/acsaem.9b01286

https://hdl.handle.net/10356/142141

https://doi.org/10.1021/acsaem.9b01286

Vertical Silver-Silver Chloride Core-Shell Nanowire Array for Carbon Dioxide Electroreduction

Junyu Ge,[†,∥] Jun Long,[‡,∥] Zixu Sun,[†,∥] Han Feng,[Δ] Jie Hu,[§] See Wee Koh,[†] Qing Yu,[†] Jianping Xiao,[*#] Hong Li[*†,¶,⊥]

[†]School of Mechanical and Aerospace Engineering, Nanyang Technological University, 639798 Singapore.
[‡]Department of Chemistry, Zhejiang University, Hangzhou, 310027, People's Republic of China.
[Δ]Advanced Environmental Biotechnology Centre, Nanyang Environment and Water Research Institute, Nanyang Technological University, 1 Cleantech Loop, Singapore 637141, Singapore.
[§]Department of Environment and Chemistry, Yanshan University, Qinhuangdao 066004, China.
[#]State Key Laboratory of Catalysis, Dalian Institute of Chemical Physics, Chinese Academy of Sciences, Zhongshan Road 457，Dalian 116023, People's Republic of China.
[¶]Centre for Micro-/Nano-electronics (NOVITAS), School of Electrical and Electronic Engineering, Nanyang Technological University, 639798, Singapore
[⊥]CINTRA CNRS/NTU/THALES, UMI 3288, Research Techno Plaza, Singapore

ABSTRACT: The total activity of a catalyst electrode depends on specific activity of individual active site, density of active site, and the electronic coupling between catalyst and its support. A core-shell nanowire array with conductive metal core and active catalyst shell holds great promise for a catalyst electrode with high total activity. Indeed, core-shell nanowire arrays have been demonstrated in various electrocatalytic reactions; yet they are underexplored for carbon dioxide (CO_2) electroreduction. Herein, we report silver@silver chloride ($Ag@AgCl_x$) core-shell nanowire array directly imprinted on Ag foil for electrocatalytic CO_2 reduction reaction (CO_2RR).

Vertical Ag nanowire (Ag NW) array was formed directly on Ag foil surface by nanoimprinting process, leading to excellent contact between Ag substrate and Ag NWs. A facile chlorination process was employed to form a $AgCl_x$ shell on Ag NW surface. The resulting catalyst shows both high total electrode activity and high specific catalyst activity. Without *iR*-correction, the Ag@$AgCl_x$ core-shell electrode shows low onset potential, and high current density. The strong electronic coupling between $AgCl_x$ shell and Ag core results in the record-high specific CO_2RR activity to date. Our work paves the way towards manufacturing highly efficient and cost-effective electrodes for electrocatalytic CO_2 reduction.

The total activity of a catalyst electrode is more crucial than the specific activity of a catalyst material for practical applications.[1] Besides the specific activity of the catalyst material (*i.e.*, the intrinsic activity of individual active sites), the total activity of a catalyst electrode also depends on the active site density (in unit geometric area) and electronic coupling between catalyst and its support. Recent study shows that superior catalyst support can maximize the catalyst's performances by strong coupling between catalyst and its support, which facilitates electron transport to the active site.[2] Thus, ideal catalyst electrode geometry should efficiently conduct electricity to all active sites on electrode by forming strong electronic coupling between support and active sites. To this end, metal@catalyst core-shell nanowire (CSNW) electrode is very promising for achieving both high total electrode activity and high specific catalyst activity.[3] The NW array increases the active site density in unit geometry area of electrode; the catalyst shell offers highly active catalytic sites for electrochemical reaction; and the metallic core offers efficient charge transport with strong electronic coupling with active sites. Indeed, CSNW arrays have been widely employed in various electrochemical reactions, including battery and supercapacitors,[4] owing to their high total activity arising from high-surface area and efficient charge transport. Particularly, vertical CSNW arrays are widely used for photoelectrochemical water splitting due to the additional benefit of light trapping in this unique geometry.[5] However, core-shell nanowire array has not been employed for carbon dioxide electroreduction.

Carbon dioxide reduction to energy fuels holds great promise to mitigate global warming by reducing carbon emission.[6] Improving the energy efficiency of carbon dioxide reduction reaction (CO_2RR) is the key for an industrially viable CO_2 reduction process. According to the very recent techno-economic analysis, the electrochemical

CO_2RR cost is comparable to those of traditional fossil fuel-derived process only when the energy conversion efficiencies reach 60%.[7] This requirement could only be fulfilled by CO_2RR to carbon monoxide (CO) that shows energy conversion efficiency close to 60%.[8] Various metals such as gold (Au),[8a] Ag[8b] and palladium (Pd) have been reported as efficient catalysts for the electrochemical reduction of CO_2 to CO. Compared to Au and Pd, Ag is > 90 times cheaper, and >20 times more abundant; yet Ag shows comparable CO_2RR performances to that of Au and Pd. Ag surface shows favorable CO binding, but poor hydrogen binding for the competing hydrogen evolution reaction (HER), leading to active and selective CO_2RR to CO.[9] Ag is thus the most promising electrocatalyst for wide implementation of CO_2RR thanks to its high energy-conversion efficiency, high selectivity, and competitive cost-effectiveness.

Nanostructured Ag has been extensively studied for electrocatalytic CO_2RR owing to its high surface area.[10] Ag nanoparticle surfaces are active, however, the total electrode activity is inferior owing to the significant Ohmic loss arising from the inefficient charge transport inside the nanoparticle film.[10c] Nanocoral Ag film formed by chlorination also shows high activity with CO current density up to 6.6 mA/cm^2 at -0.6 V vs. RHE (with *iR*-correction), however, the thick catalyst layer results in non-optimized specific activity (162 μA/cm^2 at -0.6 V vs. RHE), *i.e.*, CO current density normalized to electrochemical surface area (ECSA).[10b] Long Ag nanowire array made by high-temperature nanoimprinting has extraordinary surface area, leading to high activity (CO current density ~ 4.5 mA/cm^2 at -0.6 V vs. RHE without *iR*-correction). Nevertheless, the specific activity of Ag NW is low for CO_2RR (18.8 μA/cm^2 at -0.6 V vs. RHE).[10e] Nanoporous Ag film via dealloying shows the state-of-the-art total electrode activity (CO current density of 16.3 mA/cm^2 at -0.6 V vs. RHE without *iR*-

correction), but the fabrication process is time consuming and costly.[10a] Putting together, it is challenging to achieve both high total electrode activity and specific catalyst activity using a facile and cost-effective fabrication process.

Herein, we report a cost-effective and scalable process to fabricate Ag@$AgCl_x$ CSNW array for electrocatalytic CO_2RR that could optimize both total electrode activity and specific catalyst activity. The catalyst electrode is made via a low-temperature nanoimprinting technique to form vertical Ag NW array directly on Ag foil followed by a quick chlorination process to convert the surface of Ag NW to thin $AgCl_x$ shell as the catalyst. The resulting Ag@$AgCl_x$ CSNW array has unique features including (1) excellent contact between Ag foil substrate and Ag NWs, (2) strong electronic coupling between $AgCl_x$ shell and Ag core, (3) superior catalytic activity from $AgCl_x$ shell. As a result, the catalyst shows supervisor total activity without *iR*-correction, including low overpotential (onset potential of -0.3 V vs. RHE), and high CO current density (5.27 mA/cm^2 at -0.6 V vs. RHE). Moreover, the catalyst also shows the highest specific activity to date for electrocatalytic CO_2RR (413 μA/cm^2 at -0.6 V vs. RHE).

The schematic of our vertical Ag@$AgCl_x$ CSNW array electrode is illustrated in Figure 1. The $AgCl_x$ shell is rich of active sites for CO_2RR, and the highly conductive Ag core facilitates efficient electron transport from electrode to nanowire. The strongly coupled $AgCl_x$ shell and Ag core leads to excellent electron transfer at the catalyst-electrolyte interface. As such, the total activity of the electrode is improved by high surface area, active catalyst surface, and strong coupling between catalyst and its support. The fabrication process of vertical Ag nanowire array is based on a direct superplastic nanoimprinting method,[11] as shown in Supporting Figure S1. A stack of

anodic aluminum oxide (AAO) mold on Ag foil was hot pressed, and the surface Ag flew into AAO mold via superplastic deformation.[12] The nanowires fabricated were thus directly rooted in the Ag foil substrate, and thus greatly facilitated the electron transport. After removal of template, the Ag NWs were chlorinated in sodium chloride solution by a simple electrochemical anodic process to covert the surface of Ag nanowires to $AgCl_x$ shell (see Experimental Section for details).[10b] The Ag foil was also chlorinated with the same process to form $Ag@AgCl_x$ foil (see Supporting Figure S2 for the morphology of Ag foil before and after chlorination). The morphology of Ag NWs and $Ag@AgCl_x$ CSNWs were characterized by scanning electron microscopy (SEM), as shown in Figure 2a,b.

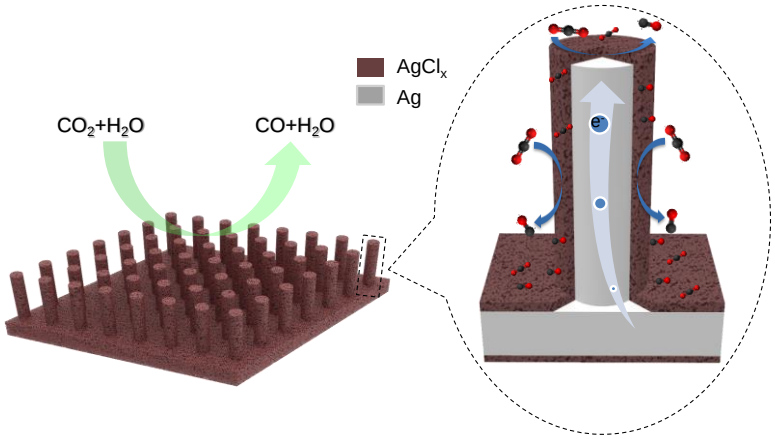

Figure 1. Schematic of $Ag@AgCl_x$ nanowire array for CO_2 reduction. Vertical Ag nanowire array is made on Ag foil by nanoimprinting. The surface of Ag nanowire array is converted to $AgCl_x$ to form a vertical $Ag@AgCl_x$ core-shell nanowire array. The $AgCl_x$ shell is active for CO_2 reduction, and the Ag core shows superior electrical conductivity. As such, the total activity of the electrode is improved by high surface area, active catalyst surface, and strong catalyst-support coupling.

The as-fabricated Ag NWs have smooth surface (Figure 2a) and high crystallinity, as confirmed by transmission electron microscopy (TEM) (Supporting Figure S3). The profile of Ag and Cl element distribution across a single Ag@$AgCl_x$ CSNW is obtained by energy-dispersive X-ray spectroscopy (EDS) line scan, as shown in Figure 2c. The higher Cl element intensity at the edges of the nanowire suggests the core-shell structure.[13] Interestingly, the $AgCl_x$ shell has small sub-10-nm nanograins (see Figure 2d), which offer rich grain boundaries for high catalytic activity.[14] Interplanar spacing of 0.277 nm and 0.320 nm correspond to (200) and (111) facets of AgCl, respectively, which are consistent with the X-ray powder diffraction (XRD) spectrum (Supporting Figure S4).[15]

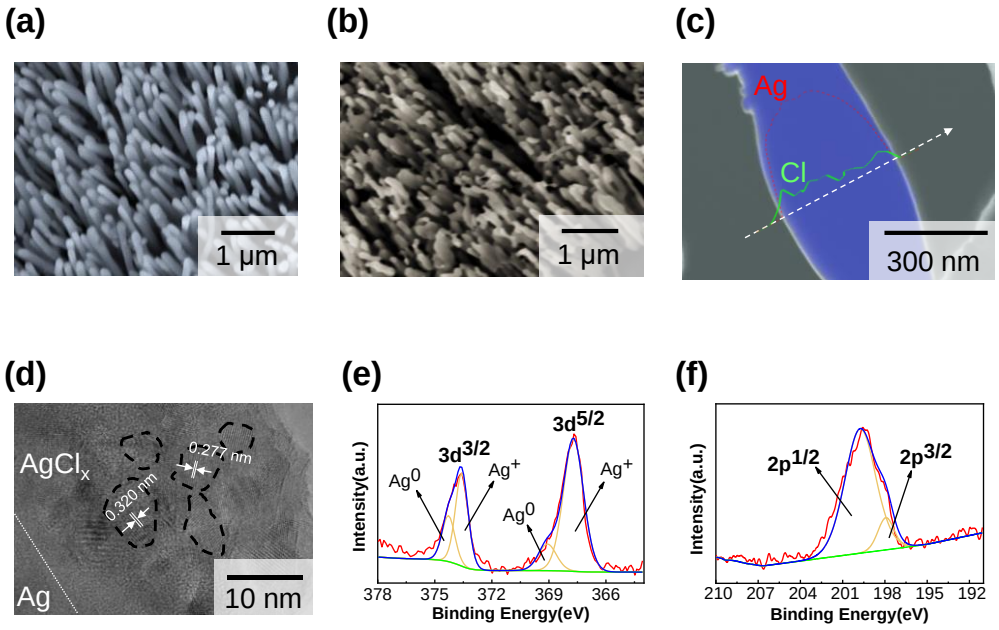

Figure 2. Characterizations of Ag NWs and Ag@$AgCl_x$ core-shell nanowires. SEM image of vertical (a) Ag and (b) Ag@$AgCl_x$ core-shell nanowires array. Scale bars of (a) and (b) are 1 μm. c) EDS line scan of a Ag@$AgCl_x$ core-shell nanowire. Inset: the intensity profiles of Ag and Cl element along the arrow. Scale bar is 300 nm. (d)

HRTEM of a Ag@$AgCl_x$ nanowire. The dashed line labels the boundary between Ag and $AgCl_x$ layer. The dashed curves indicate $AgCl_x$ particles, where the interplanar spacing of 0.277 and 0.320 nm for (200) and (111) facets of AgCl lattice are labelled. Scale bar is 10 nm. The XPS spectra of (e) Ag 3d state, and (f) Cl 2p state of Ag@$AgCl_x$ core-shell nanowire. The fitted curves are labelled with corresponding states.

The X-ray photoelectron spectroscopy (XPS) measurement was performed to further study the surface composition and the chemical state of Ag@$AgCl_x$ CSNWs. Figure 2e shows the Ag 3d state, where two peaks appear around 374 and 368 eV, respectively, and each of them can be further deconvolved into two peaks, at around 368.1/369.5 eV and 373.8 /374.5 eV. The 374.5 and 369.5 eV peaks correspond to the metallic Ag^0, and the 368.1 and 373.8 eV peaks are ascribed to ionic Ag^+.[10b] Figure 2f shows the Cl 2p state consists of two peaks at 199.7 and 198.1 eV. The derived atom ratio of Ag and Cl is about 3:1.[10b,15] A pre-electrolysis reduction of Ag@$AgCl_x$ CSNWs was conducted till a stable current level was obtained before CO_2RR to exclude the current contribution of $AgCl_x$ reduction. After electrochemical CO_2 reduction, both Ag and Cl peaks have slight shifts and atom ratio of Ag and Cl atom reduces to 10:1, as depicted in Supporting Figure S5. The reduced Ag is rich of grain boundaries and defects that are active for CO_2RR. The remaining Cl also contributes to the CO_2RR activity, which will be detailed later.

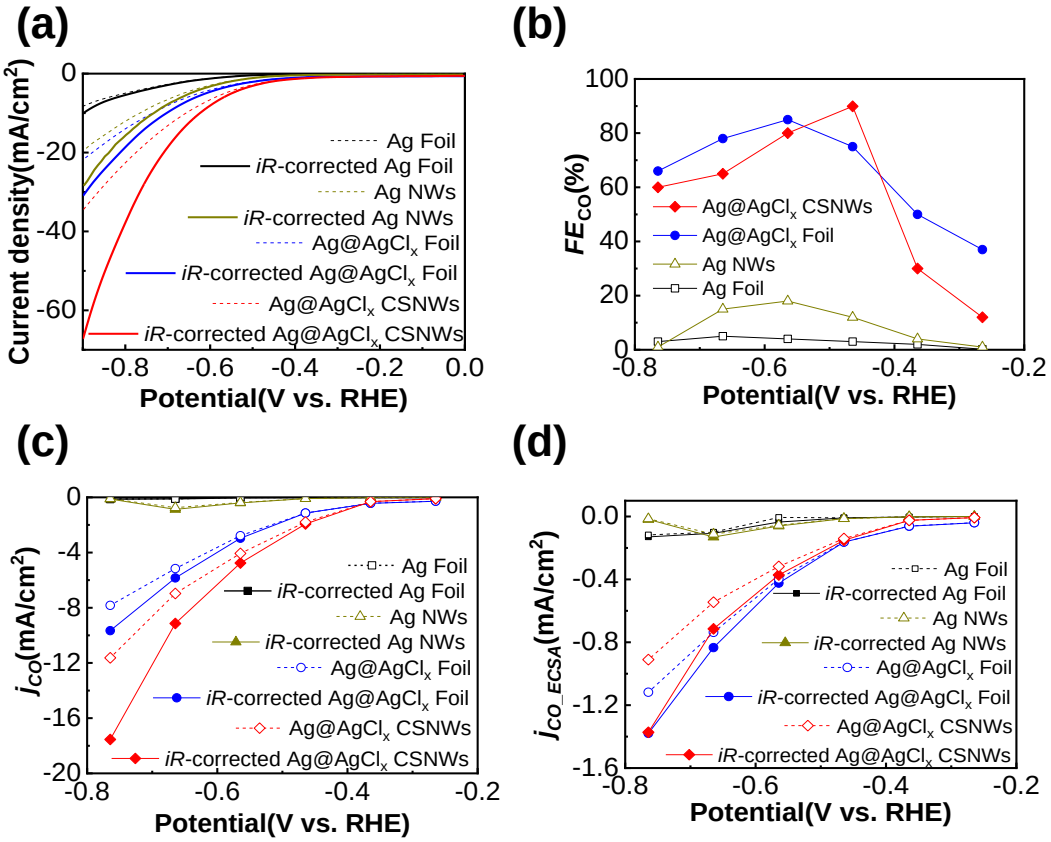

Figure 3. Electrocatalytic CO_2 reduction performance comparison among Ag@AgCl$_x$ CSNWs, Ag@AgCl$_x$ foil, Ag NWs, and Ag foil. Total electrode activity including (a) linear sweep voltammetry curves, (b) Faradaic efficiencies for CO evolution (FE_{CO}), and (c) CO partial current densities j_{CO}. (d) Specific activity of ECSA-normalized CO partial current densities j_{CO_ECSA}.

The linear sweep voltammetry (LSV) curves of Ag@AgCl$_x$ CSNWs and Ag@AgCl$_x$ foil before (dotted) and after (solid) *iR*-correction are presented in Figure 3a, along with those of pure Ag NW and Ag foil as the control samples. Ag@AgCl

$_x$ CSNWs electrode shows the highest current density with the lowest onset potential around -0.3 V vs. RHE. The faradic efficiency of CO product (FE_{CO}) is displayed in Figure 3b. FE_{CO} of Ag@AgCl$_x$ CSNWs electrode increases with applied potential and

peaks at 91% (-0.46 V vs. RHE), when the faradic efficiency of H_2 product (FE_{H2}) is only 5% (Supporting Figure S6a). In contrast, the starting material Ag foil shows FE_{CO} below 5%, and the control sample Ag NW has a FE_{CO} below 20%. It is noted that Ag@$AgCl_x$ foil has a similar FE as that of Ag@$AgCl_x$ CSNWs, suggesting that $AgCl_x$ shell dominates FE_{CO}, instead of the nanowire geometry. The high total current density (Figure 3a) and high FE_{CO} (Figure 3b) of Ag@$AgCl_x$ CSNWs lead to the high CO partial current density j_{CO}, as shown in Figure 3c. Ag@$AgCl_x$ CSNWs electrode has a j_{CO} of 6.54 (5.27) mA/cm^2 at -0.6 V vs. RHE with (without) *iR*-correction, which is 182 times higher than that of the starting Ag foil. The Ag@$AgCl_x$ foil also shows a drastically increased CO_2RR activity compared to the Ag foil (103 times higher). In obvious contrast, the Ag NW shows a poor activity with $j_{CO} < 1$ mA/cm^2 at -0.6 V vs. RHE. These comparisons suggest that $AgCl_x$ shell is rich of active sites and plays the major role of catalyst. It is worth noting that this high total electrode activity is comparable to that of Ag nanocoral (with *iR*-correction) and only less than that of nanoporous Ag (without *iR*-correction) fabricated by dealloying process (Supporting Tables S1 and S2).

To access the intrinsic/specific catalyst activity, we normalize the CO partial current density by ECSA (see Supporting Figure S7).[16] Interestingly, the ECSA-normalized CO current density j_{CO_ECSA} of Ag@$AgCl_x$ foil and CSNWs are comparable, further confirming that $AgCl_x$ dominates the catalytic activity. The total (j_{H2}) and specific H_2 current density (j_{H2_ECSA}) of Ag@$AgCl_x$ foil and Ag@$AgCl_x$ CSNWs are much smaller than that of the Ag foil and Ag NWs (Supporting Figure S6c), suggesting the intrinsic HER activity was greatly suppressed by the chlorination process. These observations suggest that our CSNW array significantly increases the active site density without

compromising the intrinsic activity of the individual active sites. It also suggests that the catalytic activity of $AgCl_x$ is maximized thanks to the strong electronic coupling between $AgCl_x$ shell and conductive Ag core. It's worth noting that j_{CO_ECSA} of $Ag@AgCl_x$ CSNWs reaches unprecedented value of 511 (413) $\mu A/cm^2$ at -0.6 V/cm^2 with (without) *iR*-correction. These values are 3 (70) times higher than Ag nanocoral[10b] with *iR*-correction (nanoporous Ag[10a] without *iR*-correction) at the -0.6 V vs. RHE (see Supporting Tables S1 and S2). Moreover, j_{CO_ECSA} of our $Ag@AgCl_x$ CSNWs is 20 times higher than that of long vertical Ag NW.[10e]

DFT calculations were performed in order to identify the active sites in $Ag@AgCl_x$ CSNW and foil. First, we determined the catalytic activity of $AgCl_x$ shell by testing the CO adsorption on different possible models, including (100) and (111) surfaces of crystalline silver chloride, and Cl modified Ag (111) [Ag(111)_Cl] and (211) surfaces [Ag(211)_Cl]. The adsorption free energy (G_{ad_CO}) on each possible model was then compared with that on Ag (111) or (211) surface. As suggested in previous report,[17] the CO_2RR activity increases with the enhancement of CO adsorption in the right side of activity volcano, whereas decreases in the left. Hence, the structures with a medium CO adsorption (namely, stronger than pure Ag surfaces but not too strong) are the potential active sites. For AgCl (100) surface (Supporting Figure S8), G_{ad_CO} was found to be -1.24 eV, which is too strong and hard for CO desorption, while it is too weak for CO adsorption on AgCl (111) surface (0.79eV) relative to that on pure Ag [0.64 eV on (111) surface]. Hence, crystalline AgCl structure is not likely the active site of electrode $AgCl_x$ shell. In addition, a few of metallic Ag surface modification by Cl have been modelled, included Ag substitution at the surface or subsurface by Cl, interstitial Cl atom into the Ag lattice. For Ag(111)_Cl (Supporting Figure S9), as the Cl is inserted

into the fcc site of Ag layers (I-fcc), CO adsorption (G_{ad_CO} = 0.21 eV) is enhanced relative to Ag(111). For Ag(211)_Cl (Supporting Figure S10), CO adsorption is only enhanced on "I-adatom", with G_{ad_CO} stronger by about 0.2 eV. Therefore, "I-fcc" of Ag (111) and "I-adatom" of Ag (211) are the potential active sties for experimental electrodes in CO_2RR, which contribute to the superior activity of $AgCl_x$ shell. The two representative structures were then studied in details, and denoted as Ag(111)_Cl and Ag(211)_Cl, respectively.

The reaction free energies (ΔG) of four elementary steps for CO_2RR to CO were analyzed and shown in Figure 4a,b. The CO_2RR activity shows a volcano trend with respect to G_{ad_CO} for both (111) and (211) surfaces. On the left side of volcano, CO desorption is the ΔG -limiting step. On the right side, however, the overall reaction is limited by CO_2 protonation, which is consistent with the previous study.[17] The ΔG-limiting step reduces on Ag(111)_Cl [Ag(211)_Cl] by 0.32 eV (0.16 eV) relative to Ag(111) [Ag(211)], indicating Ag(111)_Cl and Ag(211)_Cl are more active than pure Ag(111) and Ag(211), respectively. It is in agreement with the experimental results that the CO partial current densities on Ag@$AgCl_x$ CSNWs and Ag@$AgCl_x$ foil are much higher than the corresponding pure Ag electrodes (Figure 3d). The superior activities of Ag(111)_Cl and Ag(211)_Cl can be attributed to the more favorable adsorption of *COOH. The *COOH is adsorbed on the low-coordinated Ag atom on Ag(111)_Cl and Ag(211)_Cl, which are more reactive than the high-coordinated Ag in Ag(111) and (211) surfaces and can bind COOH stronger (Insets of Figure 4c,d). In addition, we also studied the HER performance of Cl modified Ag, which is the major competing reaction of CO_2RR. The adsorption free energy of H (G_{ad_H}) on transition metals is shown as the green line in Figure 4a,b. As shown, the H adsorption on Ag(111)_Cl and Ag(211)_Cl

deviates greatly from the unmodified transition metals with a much weaker adsorption energy. In addition, the stronger CO adsorption energies can lower the H* coverage, which suggests the HER can be suppressed significantly on Cl modified Ag shell.

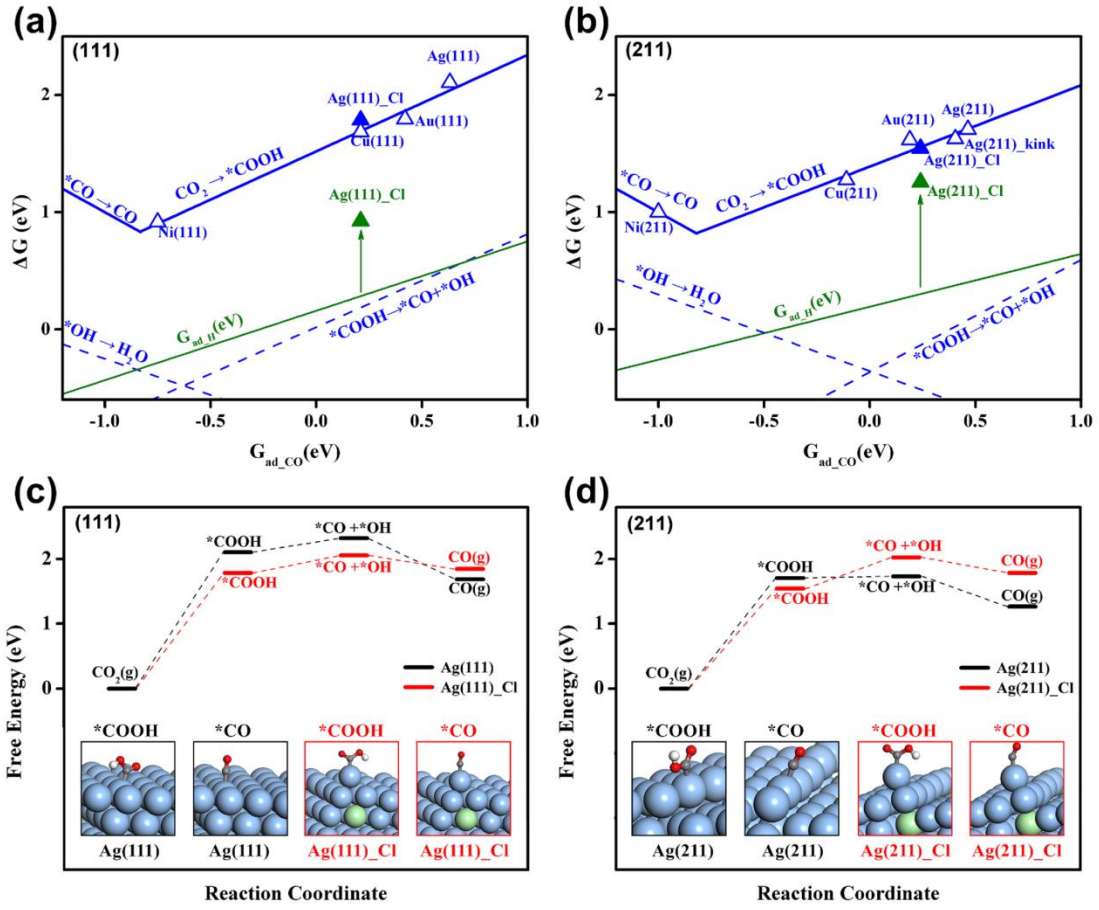

Figure 4. Reaction free energy of involved elementary step plotted as G_{ad_CO} for (a) Ag(111) and (b) Ag(211) surfaces. Blue lines represent the elementary steps in CO_2 reduction into CO. Green and lines represent the adsorption of H. Free energy profiles for CO_2RR into CO on (c) Ag(111) and Ag(111)_Cl, (d) Ag(211) and Ag(211)_Cl. Inserts are the geometric structures of *COOH and *CO. Blue and green atoms are Ag and Cl, respectively.

In conclusion, we demonstrated both high total electrode activity and high specific catalyst activity for CO_2 electroreduction using $Ag@AgCl_x$ core-shell nanowire array electrode. The nanowire array directly imprinted on Ag foil substrate shows excellent nanowire-substrate contact facilitating electron transport, and the chlorinated Ag nanowire surface exhibits high activity arising from the strong electronic coupling between catalyst and support. These features lead to efficient electron transfer to abundant active sites. Prior to *iR*-correction, the catalyst electrode shows low onset potential of -0.3 V vs. RHE, high CO current density (5.27 mA/cm^2 at -0.6 V vs. RHE), as well as record-high specific CO_2RR activity (413 $\mu A/cm^2$ normalized to ECSA at -0.6 V vs. RHE) to date. The complementary theoretical study suggests that the inserted Cl subsurface atoms in Ag lattice are responsible for the high activity, as well as the high selectivity (by suppressing the competing HER). Our work offers an efficient and cost-effective electrode for electrocatalytic CO_2 reduction.

EXPERIMENTAL SECTION

Materials preparation.

Ag NWs: Ag foil with the purity of 99.999% was washed by immersion and sonication for 15 mins in acetone, Isopropyl alcohol, ethanol, and DI water, sequentially. For fabrication of Ag NWs, firstly, an anodic aluminum oxide (AAO) template was placed on Ag foil between two press plates and heated to 300 °C. Second, a pressure of 7,800 psi was applied on the press plates which extruded Ag into the nanopores of the AAO template. After the sample was cooled to room temperature, the AAO template was removed using 1 M KOH solution to expose the nanowires.

Ag@$AgCl_x$ core-shell NWs: The Ag@$AgCl_x$ CSNWs were prepared by oxidizing Ag NWs in 0.5 M Ar-saturated NaCl solution at 10 mA/cm^2 for 30 seconds and followed by pre-reducing at -20 mA/cm^2 for 10 seconds before CO_2 reduction.

Materials Characterization: SEM images and corresponding element mapping were obtained using JEOL 7600F. XRD patterns were used for phase characterization by Panalytical X'Pert Pro. TEM images and corresponding element mapping were obtained by FEI, America and JEOL-2010HR, Japan.

Electrochemical measurements. Electrochemical experiments were conducted in a customized H-cell, separated by an ion exchange membrane (AMV from AGS, Japan). Certain amounts of $KHCO_3$ (99.7%, Sigma-Aldrich) was dissolved in Millipore water (18.2 MΩ·cm) to prepare the 0.5 M electrolyte. A pre-electrocatalysis process was conducted for 24 hours to remove contaminants in the electrolyte. Before reaction, the electrolyte was purged continuously with CO_2 for 30 minutes. A Pt wire (Sigma-Aldrich, 99.99%) was used as counter electrode and Ag/AgCl as reference electrode.

Product analysis: CO_2 reduction experiments were started by a chronoamperometric step applied by a BioLogic VMP3 workstation. After 30 minutes of electrocatalysis at constant potential, a sample of gas was analyzed by gas chromatography (Agilent 9860B) to detect the products.

Computational details. DFT calculations were conducted using the Vienna Ab initio Simulation Package (VASP),[18] and the revised Perdew-Burke-Ernzerhof (rPBE)[19] functional was used to perform all the total energy calculations. Flat (111) and step (211) surfaces of Ag were selected to study the thermodynamics of CO_2RR to CO, with the periodicity of 3×3 and 3×4, respectively. In addition, the Cl modified Ag(111) and Ag(211) was also considered to model the $AgCl_x$ shell. The adsorption of COOH, CO, OH and H were optimized on those surfaces with the Monkhorst-Pack k-point 3×3×1. 4-layers surfaces were used with two layers fixed at the bottom. All the total energy optimizations were conducted with the Plane-wave cut-off energy 400 eV and the convergence of force 0.03 $eV \cdot Å^{-1}$.

ASSOCIATED CONTENT

Supporting Information. Details of characterizations, electrochemical measurements and DFT calculations.

AUTHOR INFORMATION

Corresponding Authors

*E-mail: xiao@dicp.ac.cn.

*E-mail: ehongli@ntu.edu.sg.

Author Contributions

‖ J.G., L.J., and S.X. contributed equally to this work.

Notes

The authors declare no competing financial interest.

ACKNOWLEDGMENT

This work was supported by Nanyang Technological University under NAP award (M408050000) and Singapore Ministry of Education Tier 1 program (2018-T1-001-051). J.X. acknowledges the financial support from National Natural Science Foundation of China (21802124 and 91845103). SEM, TEM, and XRD characterizations were performed at the Facility for Analysis, Characterization, Testing and Simulation (FACTS), Nanyang Technological University, Singapore.

REFERENCES

1. Benck, J. D.; Hellstern, T. R.; Kibsgaard, J.; Chakthranont, P.; Jaramillo, T. F., Catalyzing the Hydrogen Evolution Reaction (HER) with Molybdenum Sulfide Nanomaterials. *ACS Catal*. **2014,** *4* (11), 3957-3971.

2. Voiry, D.; Fullon, R.; Yang, J.; de Carvalho Castro e Silva, C.; Kappera, R.; Bozkurt, I.; Kaplan, D.; Lagos, M. J.; Batson, P. E.; Gupta, G.; Mohite, Aditya D.; Dong, L.; Er, D.; Shenoy, V. B.; Asefa, T.; Chhowalla, M., The role of electronic coupling between substrate and 2D MoS_2 nanosheets in electrocatalytic production of hydrogen. *Nat. Mater.* **2016,** *15*, 1003.

3. Xia, X.; Tu, J.; Zhang, Y.; Wang, X.; Gu, C.; Zhao, X.-b.; Fan, H. J., High-Quality Metal Oxide Core/Shell Nanowire Arrays on Conductive Substrates for Electrochemical Energy Storage. *ACS Nano* **2012,** *6* (6), 5531-5538.

4. (a) Lu, C.; Fan, Y.; Li, H.; Yang, Y.; Tay, B. K.; Teo, E.; Zhang, Q., Core–shell CNT–Ni–Si nanowires as a high performance anode material for lithium ion batteries. *Carbon* **2013,** *63*, 54-60; (b) Gu, Z.; Nan, H.; Geng, B.; Zhang, X., Three-dimensional $NiCo_2O_4$@$NiMoO_4$ core/shell nanowires for electrochemical energy storage. *J. Mater. Chem. A* **2015,** *3* (22), 12069-12075.

5. (a) Rao, P. M.; Cai, L.; Liu, C.; Cho, I. S.; Lee, C. H.; Weisse, J. M.; Yang, P.; Zheng, X., Simultaneously Efficient Light Absorption and Charge Separation in WO_3/$BiVO_4$ Core/Shell Nanowire Photoanode for Photoelectrochemical Water Oxidation. *Nano Lett.* **2014,** *14* (2), 1099-1105; (b) Yang, J.; Bao, C.; Yu, T.; Hu, Y.;

Luo, W.; Zhu, W.; Fu, G.; Li, Z.; Gao, H.; Li, F.; Zou, Z., Enhanced Performance of Photoelectrochemical Water Splitting with ITO@α-Fe_2O_3 Core–Shell Nanowire Array as Photoanode. *ACS Appl. Mater. Interfaces* **2015,** *7* (48), 26482-26490; (c) Chakthranont, P.; Hellstern, T. R.; McEnaney, J. M.; Jaramillo, T. F., Photocatalysis: Design and Fabrication of a Precious Metal-Free Tandem Core–Shell p+n Si/W-Doped $BiVO_4$ Photoanode for Unassisted Water Splitting. *Adv. Energy Mater.* **2017,** *7* (22), 1701515; (d) Lee, B. R.; Lee, M. G.; Park, H.; Lee, T. H.; Lee, S. A.; Bhat, S. S. M.; Kim, C.; Lee, S.; Jang, H. W., All-Solution-Processed WO_3/$BiVO_4$ Core–Shell Nanorod Arrays for Highly Stable Photoanodes. *ACS Appl. Mater. Interfaces* **2019,** 11, 22, 20004-20012.

6. (a) Hollander, J.; Spialter, L., The reduction of carbon dioxide. *J. Chem. Educ.* **1958,** *35* (9), 446; (b) Kumar, B.; Llorente, M.; Froehlich, J.; Dang, T.; Sathrum, A.; Kubiak, C. P., Photochemical and Photoelectrochemical Reduction of CO_2. *Annu. Rev. Phys. Chem.* **2012,** *63* (1), 541-569; (c) Chen, C.; Khosrowabadi Kotyk, J. F.; Sheehan, S. W., Progress toward Commercial Application of Electrochemical Carbon Dioxide Reduction. *Chem.* **2018,** *4* (11), 2571-2586.

7. De Luna, P.; Hahn, C.; Higgins, D.; Jaffer, S. A.; Jaramillo, T. F.; Sargent, E. H., What would it take for renewably powered electrosynthesis to displace petrochemical processes? *Science* **2019,** *364* (6438), eaav3506.

8. (a) Verma, S.; Hamasaki, Y.; Kim, C.; Huang, W.; Lu, S.; Jhong, H.-R. M.; Gewirth, A. A.; Fujigaya, T.; Nakashima, N.; Kenis, P. J. A., Insights into the Low Overpotential Electroreduction of CO_2 to CO on a Supported Gold Catalyst in an Alkaline Flow Electrolyzer. *ACS Energy Lett.* **2018,** *3* (1), 193-198; (b) Dufek, E. J.;

Lister, T. E.; Stone, S. G.; McIlwain, M. E., Operation of a Pressurized System for Continuous Reduction of CO2. *J. Electrochem. Soc.* **2012,** *159* (9), F514-F517.

9. Hatsukade, T.; Kuhl, K. P.; Cave, E. R.; Abram, D. N.; Jaramillo, T. F., Insights into the electrocatalytic reduction of CO_2 on metallic silver surfaces. *Phys. Chem. Chem. Phys.* **2014,** *16* (27), 13814-13819.

10. (a) Lu, Q.; Rosen, J.; Zhou, Y.; Hutchings, G. S.; Kimmel, Y. C.; Chen, J. G.; Jiao, F., A selective and efficient electrocatalyst for carbon dioxide reduction. *Nat. Commun.* **2014,** *5*, 3242; (b) Hsieh, Y.-C.; Senanayake, S. D.; Zhang, Y.; Xu, W.; Polyansky, D. E., Effect of Chloride Anions on the Synthesis and Enhanced Catalytic Activity of Silver Nanocoral Electrodes for CO_2 Electroreduction. *ACS Catal.* **2015,** *5* (9), 5349-5356; (c) Kim, C.; Jeon, H. S.; Eom, T.; Jee, M. S.; Kim, H.; Friend, C. M.; Min, B. K.; Hwang, Y. J., Achieving Selective and Efficient Electrocatalytic Activity for CO_2 Reduction Using Immobilized Silver Nanoparticles. *J. Am. Chem. Soc.* **2015,** *137* (43), 13844-13850; (d) Daiyan, R.; Lu, X.; Ng, Y. H.; Amal, R., Highly Selective Conversion of CO_2 to CO Achieved by a Three-Dimensional Porous Silver Electrocatalyst. *ChemistrySelect* **2017,** *2* (3), 879-884; (e) Luan, C.; Shao, Y.; Lu, Q.; Gao, S.; Huang, K.; Wu, H.; Yao, K., High-Performance Carbon Dioxide Electrocatalytic Reduction by Easily Fabricated Large-Scale Silver Nanowire Arrays. *ACS Appl. Mater. Interfaces* **2018,** *10* (21), 17950-17956; (f) Ma, M.; Liu, K.; Shen, J.; Kas, R.; Smith, W. A., In Situ Fabrication and Reactivation of Highly Selective and Stable Ag Catalysts for Electrochemical CO_2 Conversion. *ACS Energy Lett.* **2018,** *3* (6), 1301-1306.

11. Liu, Z., One-step fabrication of crystalline metal nanostructures by direct nanoimprinting below melting temperatures. *Nat. Commun.* **2017,** *8*, 14910.

12. (a) McFadden, S. X.; Mishra, R. S.; Valiev, R. Z.; Zhilyaev, A. P.; Mukherjee, A. K., Low-temperature superplasticity in nanostructured nickel and metal alloys. *Nature* **1999,** *398* (6729), 684-686; (b) Kaibyshev, O. A., Fundamental aspects of superplastic deformation. *Mater. Sci. Eng.: A* **2002,** *324* (1), 96-102.

13. (a) Ji, X.; Yang, X.; Du, W.; Pan, H.; Luo, S.; Ji, H.; Xu, H.; Yang, T., InAs/GaSb core–shell nanowires grown on Si substrates by metal–organic chemical vapor deposition. *Nanotechnology* **2016,** *27* (27), 275601; (b) Shi, D.; Chen, J.; Riaz, S.; Zhou, W.; Han, X., Controlled nanostructuring of multiphase core–shell nanowires by a template-assisted electrodeposition approach. *Nanotechnology* **2012,** *23* (30), 305601; (c) Afsal, M.; Wang, C.-Y.; Chu, L.-W.; Ouyang, H.; Chen, L.-J., Highly sensitive metal–insulator–semiconductor UV photodetectors based on ZnO/SiO_2 core–shell nanowires. *J. Mater. Chem.* **2012,** *22* (17), 8420-8425.

14. (a) Li, C. W.; Ciston, J.; Kanan, M. W., Electroreduction of carbon monoxide to liquid fuel on oxide-derived nanocrystalline copper. *Nature* **2014,** *508*, 504; (b) Verdaguer-Casadevall, A.; Li, C. W.; Johansson, T. P.; Scott, S. B.; McKeown, J. T.; Kumar, M.; Stephens, I. E. L.; Kanan, M. W.; Chorkendorff, I., Probing the Active Surface Sites for CO Reduction on Oxide-Derived Copper Electrocatalysts. *J. Am. Chem. Soc.* **2015,** *137* (31), 9808-9811; (c) Mariano, R. G.; McKelvey, K.; White, H. S.; Kanan, M. W., Selective increase in CO_2 electroreduction activity at grain-boundary surface terminations. *Science* **2017,** *358* (6367), 1187.

15. Han, C.; Ge, L.; Chen, C.; Li, Y.; Zhao, Z.; Xiao, X.; Li, Z.; Zhang, J., Site-selected synthesis of novel Ag@ AgCl nanoframes with efficient visible light induced photocatalytic activity. *J. Mater. Chem. A* **2014,** *2* (31), 12594-12600.

16. Savinell, R. F.; Zeller, R. L.; Adams, J. A., Electrochemically Active Surface Area: Voltammetric Charge Correlations for Ruthenium and Iridium Dioxide Electrodes. *J. Electrochem. Soc.* **1990,** *137* (2), 489-494.

17. Mistry, H.; Choi, Y. W.; Bagger, A.; Scholten, F.; Bonifacio Cecile, S.; Sinev, I.; Divins Nuria, J.; Zegkinoglou, I.; Jeon Hyo, S.; Kisslinger, K.; Stach Eric, A.; Yang Judith, C.; Rossmeisl, J.; Roldan Cuenya, B., Enhanced Carbon Dioxide Electroreduction to Carbon Monoxide over Defect-Rich Plasma-Activated Silver Catalysts. *Angew. Chem. Int. Ed.* **2017,** *56* (38), 11394-11398.

18. (a) Kresse, G.; Furthmuller, J., Efficient iterative schemes for ab initio total-energy calculations using a plane-wave basis set. *Phys. Rev. B* **1996,** *54* (16), 11169-11186; (b) Kresse, G.; Furthmuller, J., Efficiency of ab-initio total energy calculations for metals and semiconductors using a plane-wave basis set. *Comput. Mater. Sci.* **1996,** *6* (1), 15-50.

19. Perdew, J. P.; Burke, K.; Ernzerhof, M., Generalized gradient approximation made simple. *Phys. Rev. Lett.* **1996,** *77* (18), 3865-3868.